Article

Tomographic Absorption Spectroscopy for H$_2$O Transport in a Laminar Jet with Inverse Concentration Gradient

Kin-Pang Cheong [1],[*], Dingfeng Shi [1], Shaotong Liu [1], Junjun Wu [2],[*], Kun Duan [3], Yong Song [4] and Wei Ren [3]

1   School of Aeronautics and Astronautics, Sichuan University, Chengdu 610065, China
2   Key Laboratory of Low-Grade Energy Utilization Technologies and Systems and School of Energy and Power Engineering, Chongqing University, Chongqing 400044, China
3   Department of Mechanical and Automation Engineering, The Chinese University of Hong Kong, Shatin, N.T., Hong Kong SAR, China
4   Sichuan Aerospace Zhongtian Power Equipment Co., Ltd., Chengdu 610199, China
*   Correspondence: kpcheong@scu.edu.cn (K.-P.C.); jjwu@cqu.edu.cn (J.W.)

Abstract: We report a tomographic absorption spectroscopy (TAS) study of water vapor transport in a laminar jet issuing into the ambient. The jet was generated using compressed dry air that was straightened by a honeycomb and a smooth contraction nozzle. A TAS scheme using the water vapor in the ambient as absorbing species and the absorption line near 1368.598 nm was proposed to study the H$_2$O transport in the laminar jet with an inverse concentration gradient. One-dimensional tomography was conducted at various heights above the nozzle, and the results were validated by the predictions from computational fluid dynamics (CFD) simulations. Particularly, the variations in the concentration gradient in the shear layer at different heights were captured. The 2D distribution of water concentration in the dry laminar jet was obtained experimentally. The present study shows that TAS has great potential in the research of mass transfer and scalar field of gaseous flows.

Keywords: tomographic absorption spectroscopy (TAS); tunable diode laser absorption spectroscopy (TDLAS); species transport; diffusion; laminar jet flow

1. Introduction

The precise sensing of gaseous processes that involve diffusion and transport, in either reactive or non-reactive flows, is important for both scientific research and engineering applications. Particularly, in the context of global warming and atmospheric pollution, the emissions of greenhouse and hazardous gases in industrial production, transportation and propulsion require accurate and long-term monitoring and effective reduction. The emission monitoring can be accomplished by the novel sensing technologies that have emerged from the fast development of laser sensors and detection principles in the past decades [1,2], which obtain the gas states (temperature, concentration, pressure, etc.) by interpreting the spectrum induced by the interaction of gaseous molecules and laser photons. Among them, tunable diode laser absorption spectroscopy (TDLAS) attracts extensive attention in environmental sensing and combustion diagnostics due to its *in situ*, fast and highly quantitative measurement, yet compact and simple optical setups [3–5].

TDLAS has promoted combustion research in many ways, including combustion chemistry (uniform condition) [6] and reaction field (non-uniform condition) [7] measurements. The line-of-sight (LOS) nature and fast temporal response of TDLAS make it extremely suitable for extracting the reaction rate parameters from uniform combustion within the shock tube [6]. Unfortunately, this LOS nature also hinders its application in non-uniform flames until it is combined with computed tomography (CT), which resulted in tomographic absorption spectroscopy (TAS). To date, detailed measurements of various flames, from axisymmetric laminar flames [8,9] to turbulent jet engine tail flames [10], from one-dimensional (1D) to three-dimensional (3D) [11–14], from single parameter of

temperature to multi-physicochemical parameters [15–18], have been demonstrated by TAS. By using hyperspectral absorption tomography, Ma et al. [10] reported the first 2D imaging of temperature and H_2O concentration fields of the J58 aero-engine with a spatial resolution of 36.3 mm and a temporal resolution up to 50 kHz. Senders et al. [17] investigated the combustion fields of two hybrid rocket injectors by simultaneously measuring the temperature, CO, CO_2 and H_2O distributions using TAS, which showed the capability of TAS in combustion performance evaluation and optimization. Wei et al. [13] extended TAS to 3D imaging with the assistance of a high-speed infrared camera, revealing the volumetric distributions of temperature, CO and CO_2 of two laminar flames by collecting absorption information from limited angles.

Despite its capability in multi-dimensional and multi-parameter measurements, TAS still faces various challenges that have been pointed out by previous studies [19–24]. The ill-posed nature of tomography requires regularized spectral reconstruction [19] and a well-arranged setup of beam grid [20]. With the help of machine learning, the reconstructed error during reconstruction can be mitigated [25,26]. It is also found that the reliability and accuracy of TAS depend on the selection of absorption transitions when the target field involves a wide range of temperatures [21,22]. Moreover, although it still needs further investigation, the flow state of the target field is found to have an additional influence on LAS measurement [23,24], which may lead to unexpected errors in TAS. It should be pointed out that the accuracy of spectral parameters in a database such as HITRAN [27] or HITEMP [28] has essential importance to the final results of TAS. In practice, most of these parameters need to be calibrated [29] to ensure a reasonable reconstruction of the unknown distributions [9]. This may be because the complicated interactions between the molecules and line mixing phenomenon at high temperature/high pressure under combustion environment lead to deviations from the standard model that is applied to obtain the spectroscopic parameters. Therefore, it is necessary to decouple the above-mentioned influences on TAS, especially the influence of fluid flow.

To address the above issues, different from previous TAS studies in complex combustion, we built a jet flow TAS platform, which is designed to conduct TAS in a non-reactive jet flow with various conditions in flow state (laminar or turbulent), species composition (single or multiple absorption species), and temperature (room or high temperature). In this way, the influences of these complex conditions under combustion environment can be decoupled and clarified, which might result in a new theory or method of absorption spectroscopy for combustion diagnostics. The present study is one of the serial investigations into advanced laser absorption spectroscopy for flow systems. On the other hand, by applying TAS to non-reactive fluid flow at room temperature, new technologies for fluid research may be developed. To the best of our knowledge, this is the first TAS study on a non-reactive, dry (comparing to the ambient), laminar jet flow at room temperature to explore the applications of TAS in the research of mass transfer and scalar field of gaseous flow. Particularly, we use the environmental H_2O as the target absorbing species, which is detected by the transition at 1368.598 nm. In this study, a computational fluid dynamics (CFD) simulation is also performed for cross-validation. Based on the near-infrared (NIR) TAS results of the H_2O concentration distributions at different heights above a laminar jet flow, the 2D contour of H_2O diffusion with inverse concentration gradient is obtained.
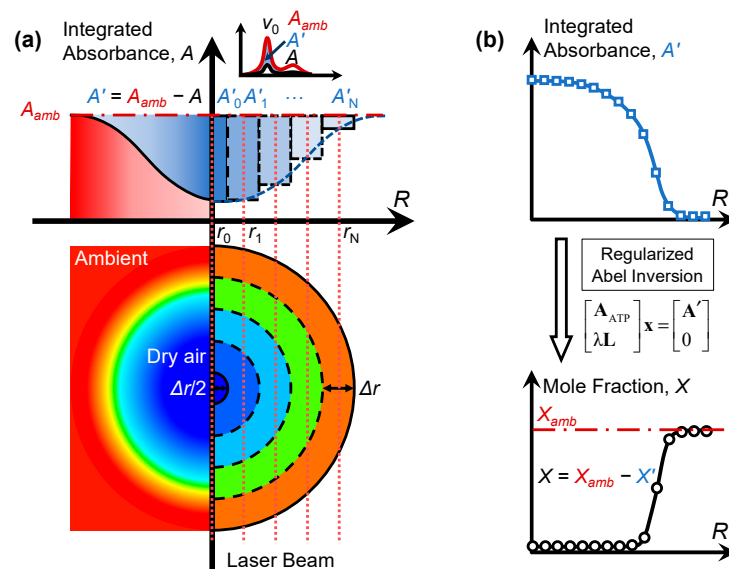
2. Methods

2.1. Theory

Figure 1 illustrates the present 1D tomography for a dry, axisymmetric, laminar jet with the inverse H_2O concentration gradient, which differs from the TAS of an axisymmetric flame or humid laminar jet with abundant H_2O molecules. The main difference is the way of extracting integrated absorbance for tomographic reconstruction and the final species concentration. Usually, for axisymmetric flows, the absorption information across the target flow is reconstructed from the measured LOS absorbance along various radial positions. Then, the local temperature or species concentration can be obtained from the reconstructed

absorption coefficients using beer's law. However, the dry laminar jet has little contribution to the LOS integrated absorbance A compared to the ambient, as shown in Figure 1. The impact of dry air can be expressed mathematically as:

$$A'_{v0}(x) = A_{v0,amb}(x) - A \tag{1}$$

where the subscript *amb* denotes ambient and v_0 denotes the line-center. The integrated absorbance can be calculated by the incident (I_0) to transmitted (I_t) laser intensities using Beer's law as:

$$A_{v0}(x) = -\int_{-\infty}^{\infty} \ln(I_t(x)/I_0(x))_v dv \tag{2}$$

Figure 1. Illustration of the present 1D tomography for a dry, axisymmetric, laminar jet with the inverse H$_2$O concentration gradient: (**a**) acquisition of LOS integrated absorbance; (**b**) reconstruction of radial species concentration using Tikhonov-regularized Abel inversion.

The impact of dry air can be written by substituting Equation (2) into (1):

$$\begin{aligned} A'_{v0}(x) &= -\left(\int_{-\infty}^{\infty} \ln\left(I_{t,amb}(x)/I_0(x)\right)_v dv - \int_{-\infty}^{\infty} \ln(I_t(x)/I_0(x))_v dv\right) \\ &= -\int_{-\infty}^{\infty} \ln\left(I_{t,amb}(x)/I_t(x)\right)_v dv \end{aligned} \tag{3}$$

For A_{v0} measured with equal spacing as shown in Figure 1, the local absorption coefficient $f(r)$ can be reconstructed with the Tikhonov-regularized three-point Abel inversion (ATP):

$$\begin{bmatrix} \mathbf{A}_{ATP} \\ \lambda\mathbf{L} \end{bmatrix} \mathbf{x} = \begin{bmatrix} \mathbf{A}' \\ 0 \end{bmatrix} \tag{4}$$

where $\mathbf{A}_{ATP}$ is the axisymmetric 1D projection matrix, $\mathbf{A}' = \{A_0, A_1, \ldots, A_N\}^T$ and $\mathbf{x} = \{f(r_1), f(r_2), \ldots, f(r_N)\}^T$ are the vectors of the measured integrated absorbance and reconstructed spectrally integrated absorption coefficient at different locations, respectively, λ is the regularization parameter that can be determined by the L-curve method [30], and $\mathbf{L}$ is a $N \times (N+1)$ smoothing matrix:

$$\mathbf{L}_{ij} = \begin{cases} 1, & \text{if } i = j \\ -1, & \text{if } i = j+1 \\ 0, & \text{otherwise} \end{cases} \tag{5}$$

After reconstructing the local integrated absorption coefficient $f(r)$, the mole fraction of the absorbing species originally in the ambient air but removed by the dry flow can be derived:

$$X'(r) = \frac{f(r)}{PS(T(r))} \qquad (6)$$

where P is the pressure and S is the temperature-dependent linestrength [1]. Finally, the actual mole fraction of the absorbing species in the flow field is:

$$X(r) = X_{amb} - X'(r) \qquad (7)$$

2.2. Experimental Setup

Figure 2 presents the schematic of the present experimental setup for investigating the H_2O transport in a dry laminar jet with TAS. As shown in Figure 2a, a near-infrared distributed-feedback (DFB) laser with the center wavelength at 1.3686 μm (69sensor, Wuhan) was utilized as the laser source, whose temperature and current were driven by a laser driver (Wavelength Electronics) with the triangle current scanning signal (1 kHz) from a function generator (Tektronix, Beaverton, OR, USA). The laser was then 50:50 split into two beams by a single mode 1×2 fused fiber coupler, one for LOS absorption measurement and the other for relative wavenumber determination with the help of a single crystal silicon etalon (FSR = 0.5 GHz). After collimation, the power of the laser beam was reduced by an iris to avoid saturation of the NIR photodetector (Thorlabs, Newton, NJ, USA). A dual-channel DAQ card (NI, PCI-6115) with a sampling rate of 10 MHz per channel was utilized for data acquisition. To reduce the disturbance of the flow while maintaining the significance of the absorption signal, the laser collimator and the photodetector were placed at a distance $L = 14$ cm, and they were installed, respectively, on two motorized linear stages (uncertainty $\pm$ 0.005 mm) and controlled simultaneously by identical preset routine. The radial stepping resolution for the present TAS measurement was $\Delta r = 1$ mm to capture the H_2O gradient within the shear layer effectively.
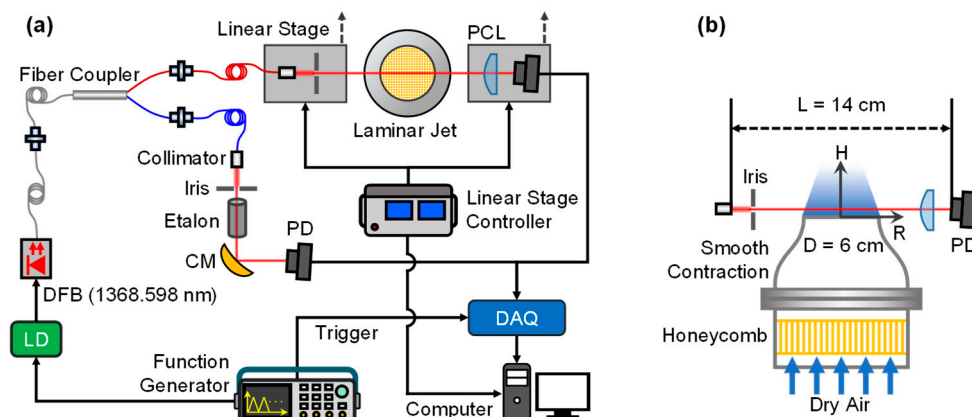
Figure 2. Schematic of the experimental setup: (**a**) optical system for the present study; (**b**) schematic of the nozzle and optical setup. CM, concave mirror; DFB, distributed-feedback laser; LD, laser driver; PCL, plano-convex lens; PD, photodetector; DAQ, data acquisition.

Figure 2b provides the details of the laminar jet nozzle. Compressed air from gas cylinders (purity of 99.8%) was controlled by mass flow controllers (Sevenstar Co., Beijing, uncertainty $\pm$ 0.5%) with a flow rate of 60 L/min. Before injecting vertically into the air, the dry air flow went through a honeycomb straightener and a smooth contraction nozzle to mitigate the effects of non-uniform flow and boundary layer on the laminar jet. The smooth contracting part was 3D printed by stereo lithography appearance (SLA) with a diameter of 60 mm and a 5 mm-thick wall. The curve of the nozzle was similar to that by Bouvet et al. [31]. Under these flow conditions, the Reynolds number of the laminar flow *Re* was 1317, which was selected after trials. It was found that the laminar jet was prone to

be disturbed by the ambient convection when *Re* was less than 1000, while the flow state would become turbulent when *Re* was too high. In addition, an exhaust hood was installed above the laminar jet to provide coflow for stabilization. The velocity of the ambient flow induced by the exhaust hood was estimated to be around 0.1 m/s.

During the absorption measurement, the room temperature and relative humidity were monitored by an electronic thermohydrometer ($\pm$2.5%) and the readings remained 30.8 °C and 65%, respectively. Each TAS measurement at a specific height above the nozzle *H* took about 4 min and the measurements were conducted from *H* = 1 mm to 10 mm with a resolution ΔH = 1 mm for the present laminar jet; thus, a complete measurement took about 40 min in total. Temperature *T* and pressure *P* were considered constant. Small variations in these two parameters had little impact on the measurement. Uncertainty analysis is provided in the next section.

The selection of absorption transition is important for TAS measurements [22]. In the present study, two NIR absorption transitions near 1368.598 nm were selected, whose spectroscopic parameters (frequency, wavelength, linestrength *S* and lower state energy *E''*) are listed in Table 1. Figure 3a plots the simulated LOS absorbance of the selected transitions at typical measurement conditions *P* = 1 atm, *T* = 303.3 K, X_{H2O} = 0.03, L_{amb} = 14 cm (ambient), L_{jet_on} = 8 cm (laminar jet on) based on the HITRAN2020 database [27]. By subtracting the LOS absorbance when the laminar jet is on, the impact of dry air can be obtained, as shown in Figure 3b. It is demonstrated that the absorption lines at 7306.7396 cm^{-1} and 7306.7519 cm^{-1} predominated the contribution to the total absorbance; thus, they are selected for the present study. The linestrengths of these two main absorption lines were merged into a single line by segmental fitting following Wang et al. [32], as displayed in Figure 3c.

Table 1. Main absorption lines selected for Voigt fitting.

Line Number	Frequency (cm^{-1})	Wavelength (nm)	S (296 K) (cm^{-2} atm^{-1})	E'' (cm^{-1})
1	7306.7396	1368.599	0.027500	325.3479
2	7306.7519	1368.597	0.445359	79.4964
Weighted line [1]	7306.7470	1368.598	0.472900	93.9700

[1] Following Wang et al. [32] based on HITRAN2020.
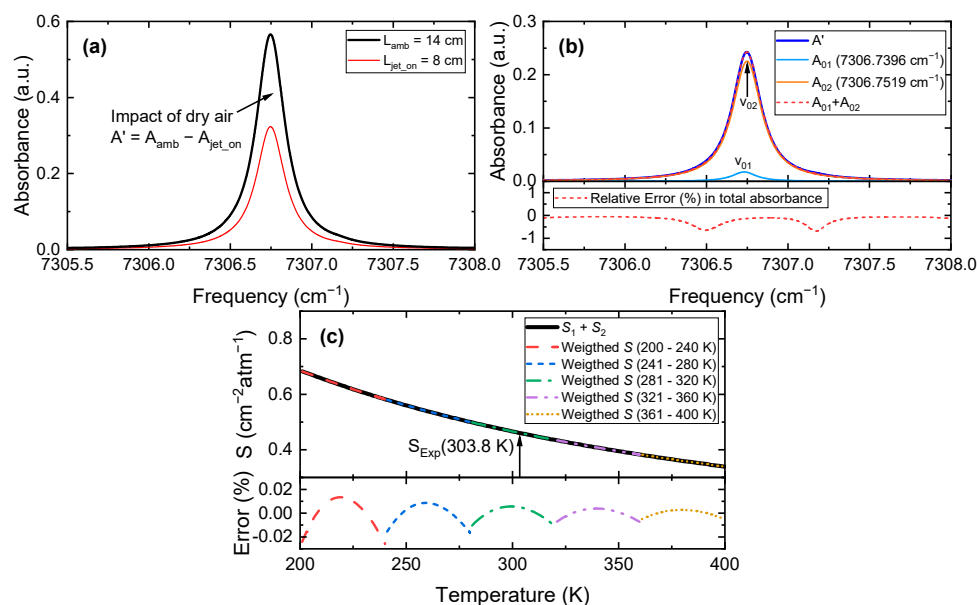
Figure 3. Simulated absorbance and linestrength of the selected transitions at typical measurement conditions: (**a**) LOS absorbances of the ambient and central position of the laminar jet; (**b**) absorbances of selected main transitions and their summation compared to the total absorbance; (**c**) merged linestrength by segmental fitting.

It is worth noting that the above optical setup allows the measurement of the species transport in a laminar jet flow by using the ambient H_2O molecules as the absorption indicator at room temperature, which may be extended to asymmetric or turbulent flow research as a new technique for the study of scalar transport and mixing of flow fields.

2.3. CFD Simulation

CFD simulation was performed for cross-validation, with the computational domain and boundary condition setups illustrated in Figure 4. The computational domain was extended to the size of 345 mm × 700 mm for simulating the laminar jet injected into the open air. By considering the axisymmetric geometry of the present flow problem, 2D axisymmetric domain and solvers were applied. The minimum grid size was set as 0.2 mm × 0.2 mm in jet core and shear layer regions with the non-uniformly growing grid in radial and downstream directions, resulting in about 110,000 cells in total. The finer grid was also tested but the variations in the result were less than 1%. Uniform velocity inlets were set for dry air and ambient air boundaries with a velocity of V_{air} = 0.3537 m/s and V_{air} = 0.1 m/s, respectively, and the corresponding H_2O mole fractions were set as 0.002 and 0.02889 according to the composition of compressed dry air and the reading of thermohydrometer. The radial boundary was set as the wall for better convergence. The kinetic-theory model was used for mass diffusivity in the species transport model. The thermodynamic and transport data for all the species were imported from the NIST database [33]. All the terms in the governing equations were second-order-discretized and the convergence criteria were 10^{-6} for all equations. The present numerical simulation was conducted using ANSYS Fluent in a 16-core workstation.
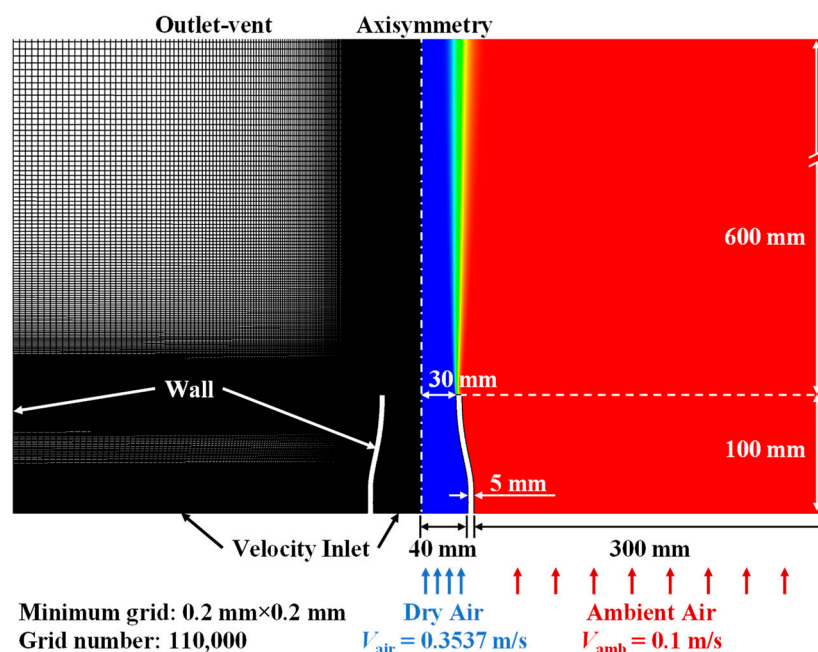

Figure 4. Numerical setup for the CFD simulation of the present laminar jet.

3. Results and Discussion

The typical raw data and etalon signal for temporal to frequency transformation are shown in Figure 5a, which were collected at H = 1 mm. To eliminate the white noise from various devices, we obtained the mean signals by averaging 100 scans, resulting in an effective temporal response of 0.1 s. By using the ambient absorption signal at r = 45 mm as the baseline, the spectral absorbances at different locations were calculated. Some representative results together with their Voigt fittings are provided in Figure 5b. It can be seen from Figure 5b that the fitting errors are generally less than 2.5%, while some wave-like signals are observed in the absorbance signals, although the raw signals are

quite smooth after averaging in Figure 5a. These wave-like signals may result from the intrinsic characteristics of the NIR DFB laser or the photodetector, or the noise from other heavy-duty devices in the laboratory. A low-pass filter with cutting frequency of 8000 Hz or averaging over more scans will mitigate these wave-like signals. However, it might result in either a change in the line shape or an increase in the experiment time. Further investigation and additional actions are needed to better mitigate this problem.
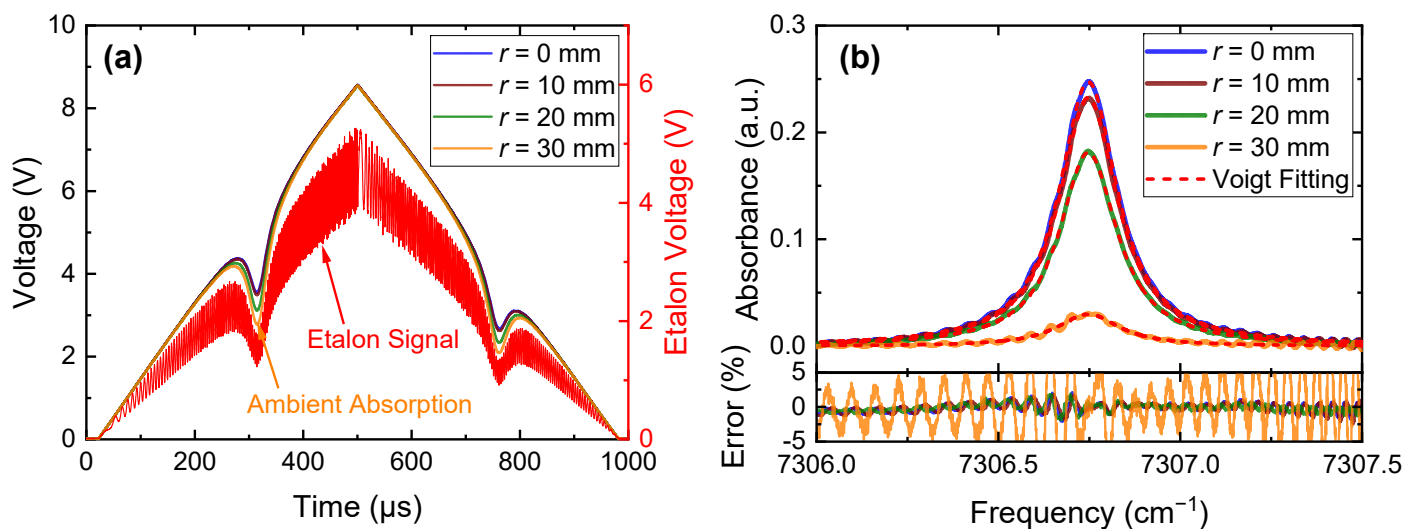
Figure 5. Typical signals and data processing for the present study: (**a**) typical raw signals and etalon signal; (**b**) absorbance and Voigt fitting at different locations, also shown are the relative errors of the fitting. These typical data are collected at $H = 1$ mm.

The LOS integrated absorbance A_{int} can be derived from the non-linear Voigt fitting process. To ensure the axisymmetry of the laminar jet, i.e., that the laminar jet was not disturbed during the measurement, the laser beam was moved from $R = -42$ mm to 42 mm to cover the nozzle and the ambient. Note that if the laminar jet is significantly disturbed by the ambient, then the distribution of A_{int} along the radial direction would be distorted away from symmetry. Typical distributions of A_{int} at different H above the nozzle are provided in Figure 6. It is shown that the original data of the measured A_{int} follow the symmetric distribution quite well, demonstrating the laminar jet was steady during the experiment, although there was a slight deviation from symmetry. Therefore, we took two additional steps for A_{int} before the tomographic reconstruction to reduce the uncertainty during the Abel inversion: (1) the symmetric mean of A_{int} was evaluated by averaging A_{int} at the same distance away from the central axis; (2) the symmetric mean of A_{int} was then smoothed using the 'sgolay' function (the Savitzky–Golay filter) with a window size of eight data points. Together with the Tikhonov regularization, the reconstruction uncertainty can be effectively suppressed.

Based on the LOS integrated absorbance A_{int} measured equidistantly, the mole fraction of H_2O X_{H2O} was reconstructed radially, as shown in Figure 7. The mole fraction gradients of H_2O in the shear layer of the laminar jet were well captured. Meanwhile, the concentrations of water vapor in the compressed air and ambient air were also obtained. Particularly, the recovered ambient X_{H2O} was very close to the measurement by the electronic thermohydrometer. In the shear layer of the laminar jet at $H = 1$ mm, discrepancies were observed between the present TAS measurement and the CFD simulation, as seen in Figure 7a. However, the variations in the X_{H2O} gradients within the shear layer when H increased from 1 mm to 9 mm, although subtle, were correctly detected by the present TAS measurements, see Figure 7b,c.
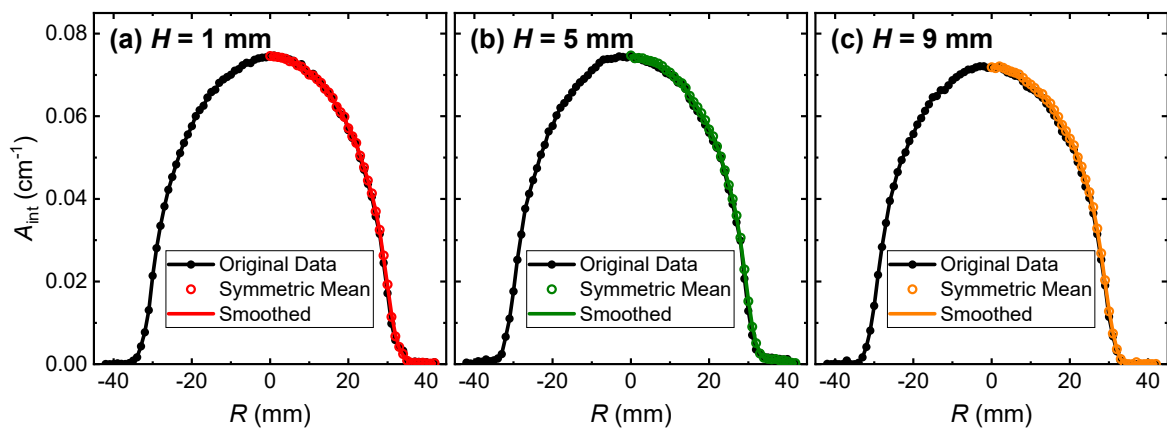
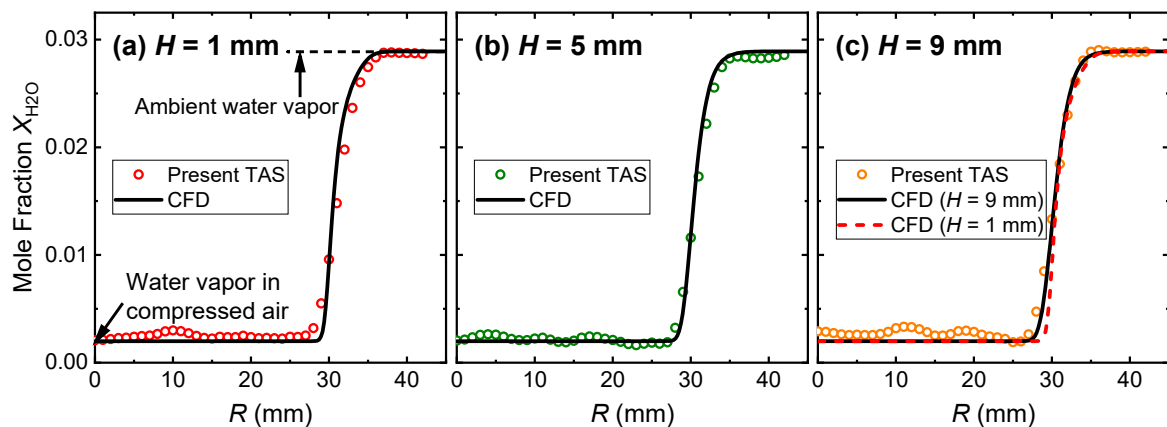**Figure 6.** LOS integrated absorbance A_{int} at different heights above the nozzle.

Figure 7. Reconstructed distributions of H_2O mole fraction X_{H2O} at different heights above the nozzle.

By combining the reconstruction at different heights, a 2D contour of H_2O mole fraction distribution is displayed in Figure 8, which is in good agreement with the CFD simulation. It can be concluded that TAS has great potential in the research of mass transfer and scalar field of gaseous flows. These results also motivate us to further explore TAS for non-reactive flow measurements in the future, from which we can develop more advanced technologies for complex reactive flows such as combustion. For unsteady flow, a time-resolved TAS measurement system is under construction.
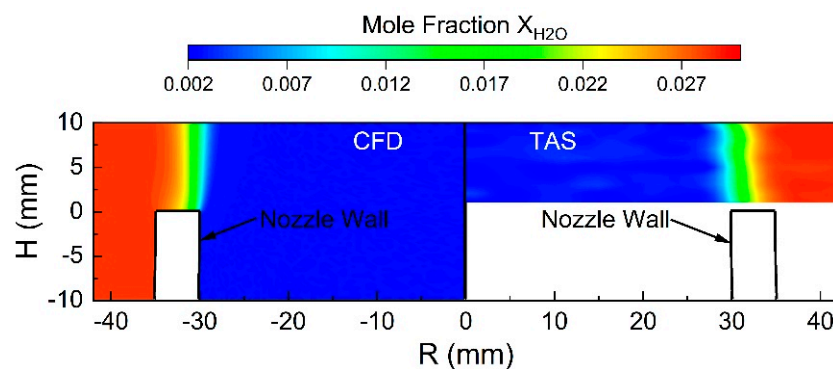

Figure 8. Two-dimensional contour of H_2O mole fraction distribution. Left, CFD simulation; right, present TAS measurement.

Since tomography was applied for the present study, the reconstruction of radial species concentrations is quite sensitive to the error/noise in the integrated absorbance. Although the distribution of the LOS A_{int} looks quite symmetric and smooth along the radial direction, the small fluctuation leads to noticeable deviations in the final reconstruction; see Figures 6 and 7. Therefore, the process to obtain A_{int}, i.e., the Voigt fitting, should account for most of the uncertainty. As we can see from Figure 5b, the uncertainty in A_{int} can be estimated as $\pm 2.5\%$. To evaluate the influence of the uncertainty in A_{int} on the final results, we ran 100 random tests with noise-perturbed A_{int} data at $H = 5$ mm. On the other hand, the uncertainty in spectral parameters such as linestrength also adds to the final result. As shown in Figure 9, the shaded area represents the 95% confidential interval of the random tests and the $\pm 2.5\%$ uncertainty in linestrength. Overall, the uncertainty of the present TAS measurement is reasonably small ($\Delta X_{H2O} \approx \pm 0.0025$) considering that we used the ambient H_2O ($X_{H2O} = 0.02889$) as the absorbing species.
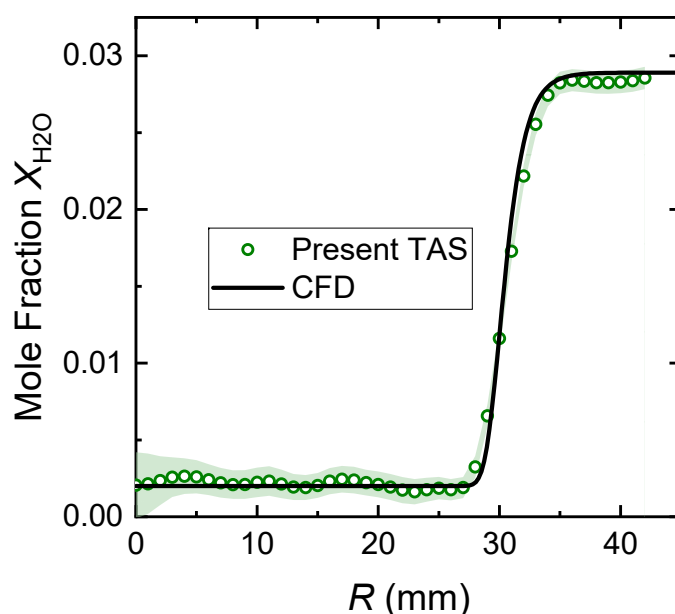
Figure 9. Uncertainty of the present TAS reconstructions of X_{H2O} ($H = 5$ mm) in the laminar jet.

4. Conclusions

In the present paper, a detailed absorption spectroscopy measurement for H_2O transport in a non-reactive laminar jet with an inverse concentration gradient was reported for the first time. The jet was generated using compressed dry air straightened by a honeycomb and a smooth contraction nozzle. To reveal the H_2O transport in a laminar jet, a tomographic absorption spectroscopy scheme was proposed by using the water vapor in the ambient as the absorbing species, and the absorption line near 1368.598 nm for sensing. One-dimensional tomography was conducted radially at $R = -42$ mm to 42 mm at various heights above the nozzle ranging from $H = 1$ mm to 10 mm. By comparing with the predictions from CFD simulations, it was confirmed that the mole fraction of water vapor X_{H2O} can be successfully reconstructed with reasonable uncertainty (± 0.0025) by the present optical system. The 2D distribution of X_{H2O} for the laminar jet was obtained experimentally using TAS, which is in good agreement with the CFD simulations. Although the signal acquisition and post-processing still need improvements, it was demonstrated that TAS has great potential in the research of mass transfer and the scalar field of gaseous flows. The present method can be further developed to apply to unsteady flows and improved technologies for combustion diagnostics might result from the present serial studies in non-reactive jets. The related work is ongoing and will be reported in the future.

References

1. Hanson, R.K.; Spearrin, R.M.; Goldenstein, C.S. *Spectroscopy and Optical Diagnostics for Gases*; Springer: Berlin/Heidelberg, Germany, 2016; ISBN 3-319-23252-5.
2. Farooq, A.; Alquaity, A.B.S.; Raza, M.; Nasir, E.F.; Yao, S.; Ren, W. Laser Sensors for Energy Systems and Process Industries: Perspectives and Directions. *Prog. Energy Combust. Sci.* **2022**, *91*, 100997. [CrossRef]
3. Hanson, R.K. Applications of Quantitative Laser Sensors to Kinetics, Propulsion and Practical Energy Systems. *Proc. Combust. Inst.* **2011**, *33*, 1–40. [CrossRef]
4. Lackner, M. Tunable Diode Laser Absorption Spectroscopy (TDLAS) in the Process Industries—A Review. *Rev. Chem. Eng.* **2007**, *23*, 65–147. [CrossRef]
5. Fu, B.; Zhang, C.; Lyu, W.; Sun, J.; Shang, C.; Cheng, Y.; Xu, L. Recent Progress on Laser Absorption Spectroscopy for Determination of Gaseous Chemical Species. *Appl. Spectrosc. Rev.* **2022**, *57*, 112–152. [CrossRef]
6. Hanson, R.K.; Davidson, D.F. Recent Advances in Laser Absorption and Shock Tube Methods for Studies of Combustion Chemistry. *Prog. Energy Combust. Sci.* **2014**, *44*, 103–114. [CrossRef]
7. Cai, W.; Kaminski, C.F. Tomographic Absorption Spectroscopy for the Study of Gas Dynamics and Reactive Flows. *Prog. Energy Combust. Sci.* **2017**, *59*, 1–31. [CrossRef]
8. Liu, C.; Xu, L.; Li, F.; Cao, Z.; Tsekenis, S.A.; McCann, H. Resolution-Doubled One-Dimensional Wavelength Modulation Spectroscopy Tomography for Flame Flatness Validation of a Flat-Flame Burner. *Appl. Phys. B Lasers Opt.* **2015**, *120*, 407–416. [CrossRef]
9. Liu, X.; Zhang, G.; Huang, Y.; Wang, Y.; Qi, F. Two-Dimensional Temperature and Carbon Dioxide Concentration Profiles in Atmospheric Laminar Diffusion Flames Measured by Mid-Infrared Direct Absorption Spectroscopy at 4.2 Mm. *Appl. Phys. B Lasers Opt.* **2018**, *124*, 61. [CrossRef]
10. Ma, L.; Li, X.; Sanders, S.T.; Caswell, A.W.; Roy, S.; Plemmons, D.H.; Gord, J.R. 50-KHz-Rate 2D Imaging of Temperature and H2O Concentration at the Exhaust Plane of a J85 Engine Using Hyperspectral Tomography. *Opt. Express* **2013**, *21*, 1152–1162. [CrossRef]
11. Liu, C.; Xu, L.; Cao, Z. Measurement of Nonuniform Temperature and Concentration Distributions by Combining Line-of-Sight Tunable Diode Laser Absorption Spectroscopy with Regularization Methods. *Appl. Opt.* **2013**, *52*, 4827–4842. [CrossRef]
12. Wei, C.; Pineda, D.I.; Paxton, L.; Egolfopoulos, F.N.; Spearrin, R.M. Mid-Infrared Laser Absorption Tomography for Quantitative 2D Thermochemistry Measurements in Premixed Jet Flames. *Appl. Phys. B* **2018**, *124*, 123. [CrossRef]
13. Wei, C.; Schwarm, K.K.; Pineda, D.I.; Spearrin, R.M. Volumetric Laser Absorption Imaging of Temperature, CO and CO_2 in Laminar Flames Using 3D Masked Tikhonov Regularization. *Combust. Flame* **2021**, *224*, 239–247. [CrossRef]
14. Qu, Z.; Fatehi, H.; Schmidt, F.M. Potassium Release from Biomass Particles during Combustion—Real-Time In Situ TDLAS Detection and Numerical Simulation. *Appl. Sci.* **2021**, *11*, 8887. [CrossRef]
15. Wang, Z.; Zhou, W.; Yan, J.; Kamimoto, T.; Tsujimoto, K.; Li, Y.; Deguchi, Y.; Sani, N.A.; Samsuri, S.H.; Zulkifli, M.F. Application of 2D Temperature Measurement to a Coal-Fired Furnace Using CT-TDLAS. *Meas. Sci. Technol.* **2020**, *31*, 035203. [CrossRef]
16. Qu, Z.; Holmgren, P.; Skoglund, N.; Wagner, D.R.; Broström, M.; Schmidt, F.M. Distribution of Temperature, H_2O and Atomic Potassium during Entrained Flow Biomass Combustion—Coupling in Situ TDLAS with Modeling Approaches and Ash Chemistry. *Combust. Flame* **2018**, *188*, 488–497. [CrossRef]
17. Sanders, I.C.; Bendana, F.A.; Hagström, C.G.; Mitchell Spearrin, R. Injector Effects on Hybrid Polymethylmethacrylate Combustion Assessed by Thermochemical Tomography. *J. Propuls. Power* **2021**, *37*, 928–943. [CrossRef]
18. Dong, M.; Zheng, C.; Miao, S.; Zhang, Y.; Du, Q.; Wang, Y.; Tittel, F. Development and Measurements of a Mid-Infrared Multi-Gas Sensor System for CO, CO_2 and CH_4 Detection. *Sensors* **2017**, *17*, 2221. [CrossRef] [PubMed]

19. Daun, K.J.; Thomson, K.A.; Liu, F.; Smallwood, G.J. Deconvolution of Axisymmetric Flame Properties Using Tikhonov Regularization. *Appl. Opt.* **2006**, *45*, 4638. [CrossRef] [PubMed]

20. Yu, T.; Tian, B.; Cai, W. Development of a Beam Optimization Method for Absorption-Based Tomography. *Opt. Express* **2017**, *25*, 5982–5999. [CrossRef]

21. Ma, L.; Li, X.; Cai, W.; Roy, S.; Gord, J.R.; Sanders, S.T. Selection of Multiple Optimal Absorption Transitions for Nonuniform Temperature Sensing. *Appl. Spectrosc.* **2010**, *64*, 1273–1282. [CrossRef]

22. Cheong, K.-P.; Ma, L.; Wang, Z.; Ren, W. Influence of Line Pair Selection on Flame Tomography Using Infrared Absorption Spectroscopy. *Appl. Spectrosc.* **2019**, *73*, 529–539. [CrossRef]

23. Ma, L.; Cheong, K.-P.; Duan, K.; Yuan, C.; Ren, W. Hybrid Constraint Multi-Line Absorption Spectroscopy for Non-Uniform Thermochemical Measurements in Axisymmetric Laminar and Jet Flames. *Opt. Lasers Eng.* **2022**, *154*, 107014. [CrossRef]

24. Wei, C.; Perakis, N.; Pineda, D.I.; Egolfopoulos, F.N.; Ihme, M.; Spearrin, R.M. Turbulence-Induced Bias in Time-Averaged Laser Absorption Tomography of Correlated Concentration and Temperature Fields with a First-Order Correction. *Combust. Flame* **2022**, *242*, 112210. [CrossRef]

25. Wang, Z.; Zhu, N.; Wang, W.; Chao, X. Y-Net: A Dual-Branch Deep Learning Network for Nonlinear Absorption Tomography with Wavelength Modulation Spectroscopy. *Opt. Express* **2022**, *30*, 2156. [CrossRef]

26. Li, H.; Ren, T.; Liu, X.; Zhao, C. U-Net Applied to Retrieve Two-Dimensional Temperature and CO_2 Concentration Fields of Laminar Diffusion Flames. *Fuel* **2022**, *324*, 124447. [CrossRef]

27. Gordon, I.E.; Rothman, L.S.; Hargreaves, R.J.; Hashemi, R.; Karlovets, E.V.; Skinner, F.M.; Conway, E.K.; Hill, C.; Kochanov, R.V.; Tan, Y.; et al. The HITRAN2020 Molecular Spectroscopic Database. *J. Quant. Spectrosc. Radiat. Transf.* **2022**, *277*, 107949. [CrossRef]

28. Rothman, L.S.; Gordon, I.E.; Barber, R.J.; Dothe, H.; Gamache, R.R.; Goldman, A.; Perevalov, V.I.; Tashkun, S.A.; Tennyson, J. HITEMP, the High-Temperature Molecular Spectroscopic Database. *J. Quant. Spectrosc. Radiat. Transf.* **2010**, *111*, 2139–2150. [CrossRef]

29. Goldenstein, C.S.; Jeffries, J.B.; Hanson, R.K. Diode Laser Measurements of Linestrength and Temperature-Dependent Lineshape Parameters of H_2O-, CO_2-, and N_2-Perturbed H_2O Transitions near 2474 and 2482nm. *J. Quant. Spectrosc. Radiat. Transf.* **2013**, *130*, 100–111. [CrossRef]

30. Hansen, P.C.; O'Leary, D.P. The Use of the L-Curve in the Regularization of Discrete Ill-Posed Problems. *SIAM J. Sci. Comput.* **1993**, *14*, 1487–1503. [CrossRef]

31. Bouvet, N. On the Simulation of Laminar Strained Flames in Stagnation Flows: 1D and 2D Approaches versus Experiments. *Combust. Flame* **2014**, *161*, 438–452. [CrossRef]

32. Wang, Z.; Wang, W.; Ma, L.; Fu, P.; Ren, W.; Chao, X. Mid-Infrared CO_2 Sensor with Blended Absorption Features for Non-Uniform Laminar Premixed Flames. *Appl. Phys. B* **2022**, *128*, 31. [CrossRef]

33. Lemmon, E.W.; Huber, M.L.; McLinden, M.O. *NIST Standard Reference Database 23. Reference Fluid Thermodynamic and Transport Properties (REFPROP)*; version 9; National Institute of Standards and Technology: Boulder, CO, USA, 2010.